ACS APPLIED MATERIALS & INTERFACES

Research Article

www.acsami.org

Binder-Free Si Nanoparticle Electrode with 3D Porous Structure Prepared by Electrophoretic Deposition for Lithium-Ion Batteries

Yang Yang, Dingqiong Chen, Bo Liu, and Jinbao Zhao*

State Key Laboratory of Physical Chemistry of Solid Surfaces, Department of Chemistry, College of Chemistry and Chemical Engineering, Collaborative Innovation Center of Chemistry for Energy Materials, Xiamen University, Xiamen 361005, China

Supporting Information

ABSTRACT: A binder-free silicon (Si) based electrode for lithium-ion battery was fabricated in an organic solvent through one-step electrophoretic deposition (EPD). The nanosized Si and acetylene black (AB) particles were bonded tightly together to form a homogeneous co-deposited film with 3D porous structure through the EPD process. The 3D porous structure provides buffer spaces to alleviate the mechanical stress due to silicon volume change during the cycling and improves lithium-ion conductivity by shortening ion diffusion length and better ion conducting pathway. The electrode prepared with 5 s deposition duration shows the best cycling performance among electrodes fabricated by EPD method, and thus, it was selected to be compared with the silicon electrode prepared by the conventional method. Our results demonstrate that the Si nanoparticle electrode prepared through EPD exhibits smaller cycling capacity decay rate and better rate capability than the electrode prepared by the conventional method.

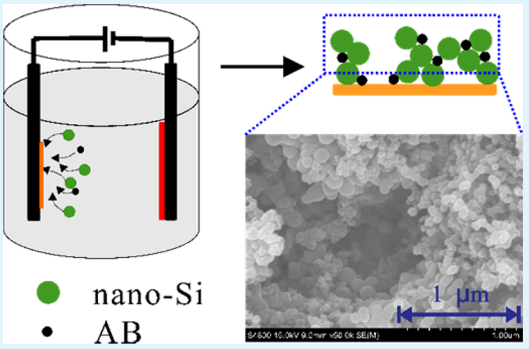

KEYWORDS: *binder-free, lithium-ion battery, Si, electrophoretic deposition, 3D porous structure*

1. INTRODUCTION

The demand of lithium-ion batteries (LIB) with high capacity from portable electronic devices and electric vehicles accelerates the development of LIB to reach its full strength. In many cases, LIB has now become the bottleneck of new technology developments. Silicon (Si) is considered as one of the most attractive materials to replace the current graphite anode (specific capacity 372 $mAh{\cdot}g^{-1}$) because of its high theoretical specific capacity (4200 $mAh{\cdot}g^{-1}$)[1] and low discharge potential (~0.4 V versus Li/Li^+). However, Si anodes undergo significant volume expansion and contraction during Li^+ insertion/extraction (~300%),[2,3] which causes the pulverization of the Si particles as well as the disconnection of electrical contact to the current collector, resulting in a rapid capacity fading.[4] Many efforts have been devoted to the preparation of various Si materials with specific structures to improve its cycling performances,[5−9] while only very few studies focus on the development of new electrode fabrication methods to improve Si anode performance.

The conventional method of fabrication of silicon nanoparticle electrode (casting a slurry containing silicon nanoparticles, conductive agents, and binders to the current collector[10]) cannot prevent silicon nanoparticle aggregation to form large particles during the mixing process, and the use of binder(s) is adverse to the enhancement of the electrode capacity because of the extra weight of inactive materials. Some binder-free methods were invented. For example, chemical vapor deposition (CVD) technique was adopted to build Si nanowire electrode[11−14] and radio frequency magnetron sputtering was employed to fabricate Si thin film electrode.[15−17] Nevertheless, these methods are expensive, difficult to scale up, and Si thin film electrodes are of low loading of active materials.

To develop a method easy to scale up for high capacity silicon electrode, especially starting from silicon nanoparticles, we consider EPD because it is one of the binder-free coating techniques with many advantages, such as short processing time, inexpensive, and industrially scalable.[18] In addition, the aggregation of nanoparticles can be eliminated because of their manageable dispersion in chosen solvent. EPD has been successfully applied to the preparation of several cathode electrodes such as $LiCoO_2$,[19] $LiMn_2O_4$,[20] and $LiNi_{0.5}Mn_{1.5}O_4$.[21] Few attempts were made to manufacture anode electrode such as SnO_2 nanoparticles and Si−CuO quantum dots by employing EPD.[22,23] In this paper, we report our work on fabrication of Si nanoparticle electrode with 3D porous structure through one-step EPD. 3D porous Si electrodes possess the structural features of both nanoscale building blocks and microsized assemblies and thus possess enhanced electrochemical performance.[24−26] Our results demonstrate that the Si nanoparticle electrode prepared through EPD shows better electrochemical performance than the electrode prepared by the conventional method.

Received: November 11, 2014
Accepted: March 27, 2015
Published: March 27, 2015

DOI: 10.1021/acsami.5b00421
ACS Appl. Mater. Interfaces 2015, 7, 7497−7504

2. EXPERIMENTAL SECTION

2.1. Materials. Nano Si powder (APS ≤ 50 nm, 98%, laser synthesized from vapor phase, Alfa Aesar), acetylene black (Guangzhou Songbai Chemical Co.,Ltd.), citric acid monohydrate (Sinopharm Chemical Reagent Co.,Ltd.), acetone (Xilong Chemical Ltd.), copper foil (United Copper Foils Ltd.), and platinum plate (Gaoss Union Science and Technology Ltd.) were used as received without further purification. Celgard 2400 was used as a separator. The electrolyte of 1.0 M $LiPF_6$ in ethylene carbonate (EC, >99.9%)/diethylene carbonate (DEC, >99.9%)/dimethyl carbonate (DMC, >99.9%) (v/v/v = 1:1:1, water content of <20 ppm) was purchased from Zhangjiagang Guotai-Huarong New Chemical Materials Company, and 5% (weight) fluoroethylene carbonate (FEC) was added before use.

2.2. Fabrication of Si Nanoparticle Electrode. In a typical preparation procedure of the electrode, 0.05 g of nano-Si, 0.05 g of citric acid monohydrate, and 0.02 g of AB were dispersed in 50 mL of acetone by the disperser (T10 basic, IKA Works GmbH & Co.) for 20 min to obtain EPD bath suspension. Citric acid monohydrate is added to convert the surfaces of nano-Si and AB to be negatively charged; thus, nano-Si and AB co-deposited film is termed as anodic EPD. As shown in Figure 1, in a standard EPD setup, a copper foil (10 μm × 2.5 cm × 2.5 cm) and a platinum plate (2 mm × 3 cm × 3 cm) were used as the anode and cathode, respectively, and the distance between the two electrodes was about 1.5 cm. EPD was performed under 120 V potentiostatic condition. In order to avoid the gravitational sedimentation of particles, the suspension was slowly stirred with a magnetic stirrer. EPD was performed in a time ranging from 5 s to 1 min. Co-deposited films are thus labeled according to their EPD duration; for example, EPD-5s is for 5 s deposition duration. The EPD co-deposited film was dried at 80 °C under vacuum condition for 12 h to obtain the final electrode. The thickness and coating density of as-prepared EPD electrodes are shown in Table 1. A comparative electrode was also prepared by the conventional method. Deionized water was employed as solvent in this case. The weight ratio (9:1) of nano-Si to AB was kept the same as that of EPD electrode. Nano-Si, AB, and 10% binder (CMC/SBR = 1:1) were mixed together to prepare the slurry. The conventional method electrode was fabricated by casting the slurry on the copper foil and dried at 80 °C under vacuum for 12 h.

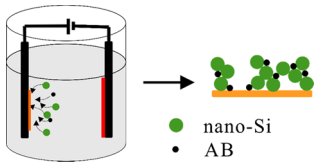

Figure 1. Schematic of process for fabrication of EPD electrode.

Table 1. Thickness and Coating Density of EPD Electrode with Different Deposition Time

sample	thickness (μm)	coating density (mg·cm^{-2})
EPD-5s	6.1	0.25
EPD-15s	15.0	0.47
EPD-30s	20.0	0.81
EPD-60s	25.6	1.1

2.3. Characterizations. The ζ potential of particles was measured on ZetaPALS ζ potential analyzer (Brookhaven Instruments Corporation). XPS experiments were carried out on a Qtac-100 LEISS-XPS system. The XRD data were collected on Rigaku miniflex 600 equipped with Cu Kα radiation operated at 40 kV and 15 mA and scanned from 10° to 90° at 1° min^{-1} with a step size of 0.02°. The structure of pristine nano-Si was examined by transmission electron microscopy (TEM, JEOL-2100). The morphologies of the EPD co-deposited film and the conventional electrode were characterized by scanning electronic microscopy (SEM, HITACHI S-4800). X-ray spectroscopy (EDS, OXFORD 7593-H) as an accessory of SEM was carried out to analyze the surface distribution of elements of the EPD co-deposited film with 20KV acceleration voltage. The AB content (carbon content) in the co-deposited film was analyzed using a VARIO EL III element analysis instrument (Elementar Co., Germany). The nano-Si content was calculated as the remaining content.

The electrochemical performance of the electrodes was tested in the form of coin cell with metal lithium foil as both counter and reference electrodes. Porous polyethylene membrane was used as the separator and 1 M $LiPF_6$ EC/DEC/DMC (v/v/v = 1:1:1) with 5% FEC as the electrolyte. The charge−discharge cycling tests were conducted on a battery cycler (Shenzhen Neware) at various current rates within the voltage range of 0.02−1.5 V (vs Li^+/Li). Cyclic voltammetry (CV) was performed on a CHI440B electrochemical workstation at a scan rate of 0.1 mV s^{-1} with the voltage range of 0.02−1.5 V (vs Li^+/Li). Electrochemical impedance spectra (EIS) tests proceeded on an electrochemical workstation of Solartron SI 1287 at a frequency range from 0.01 Hz to 100 kHz. All of the electrochemical properties were measured at 25 °C.

3. RESULTS AND DISCUSSION

The dispersing medium for EPD is of great importance for uniform film formation and can be divided into two categories: aqueous and organic systems. In general, organic liquids are superior to water as a dispersing media for electrophoretic forming due to their good chemical stability and low conductivity. In addition, the electrolysis and gas evolution associated with aqueous EPD processing can be avoided by using organic solvents of extremely high oxidation−reduction potentials.[18] Acetone is one of the representative organic dispersing medium with a low boiling point at 56.5 °C, resulting in the easy removal of the residual solvent from the co-deposited film during vacuum drying process. On the basis of the above, acetone is employed as the dispersing medium in the present work. In order to synthesize a homogeneous nano-Si and AB co-deposited film, both particles have to bear the same kind electrical charge. The surface charges of Si nanoparticle and AB in acetone were examined by ζ potential measurements. As shown in Table 2, the surfaces of Si (sample 1) and AB (sample 3) were negatively and positively charged, respectively. Citric acid is a widely used polymeric stabilizer. Through a steric stabilization mechanism, the adsorption of citrate causes a negatively charged powder surface.[27−30] As a result, after citric acid was added, the surface of modified Si (sample 2) carried more negative charge; moreover, the surface of modified AB (sample 4) was transferred to negative charge too. Afterward, the Si−AB co-deposited films are obtained by applying EPD at 120 V for 5−60 s.

Table 2. ζ Potential of Nano-Si and AB Particles in Acetone and Acetone + Citric Acid Bath

	concentration in suspension (g·L^{-1})			
sample	Si	AB	citric acid monohydrate	ζ potential (mV)
1	0.02	0	0	−13.05
2	0.02	0	0.02	−15.69
3	0	0.008	0	1.12
4	0	0.008	0.02	−7.1

The direct optical photograph of the EPD-5s film is shown in Figure 2a. Optically the film is homogeneous and its surface is very smooth, no cracks in the film are observed, all are similar

DOI: 10.1021/acsami.5b00421
ACS Appl. Mater. Interfaces 2015, 7, 7497−7504

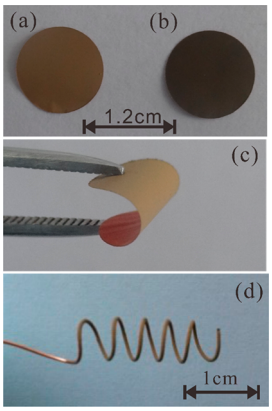

Figure 2. Photographs of (a) the EPD co-deposited film consisting of nano-Si and AB, (b) the conventional film, (c) mechanical stability test of nano-Si and AB co-deposited film and (d) the EPD co-deposited film formed on Cu wire.

to that of the conventional one (Figure 2b). The co-deposit film exhibits a good adhesion to its copper substrate; even after 100 cycles, the EPD electrode maintains good mechanical stability (Figure S1 in the Supporting Information). A bending test (Figure 2c) illustrates that the film could be easily curved without observable cracking, suggesting that EPD method is a versatile method to deposit nanoparticle film on substrates with different geometry. Figure 2d shows the photograph of the co-deposited film on Cu wire. It can be found that in both geometries (flat and curved), the deposit films are smooth without defects.

Figure 3 illustrated the TEM and SEM images of nano-Si, EPD co-deposited electrode and conventional electrode (both electrodes are not calendered). From the images of the nano-Si starting material and cross-section of the EPD co-deposited film, it is clearly seen that the particle size of nano-Si material is around 50−100 nm and the co-deposited film is approximately 6.1 μm thick. It also shows a good adhesion to copper substrate without observable gaps between film and copper foil. The side view of the film indicates that the film is smooth. Figure 3c,d shows the surface morphologies of the co-deposited film. Interconnected macropores/micropores are present in this 3D porous structure. According to the Henry equation (Supporting Information, page S-1),[18] because ζ potentials of Si and AB particles are relatively low (see Table 2), velocities of these particles are relatively small, the pressure exerted by the arriving particles enabling the particles close to the deposit is small, therefore leading to 3D porous, sponge-like deposit. This result is consistent with previous studies of other materials.[31,32] The 3D porous structure generates a large specific surface area, thus reduces diffusion length of lithium-ions, and enhances the contact area between the electrode and the electrolyte, which is also beneficial to lithium-ion transportation. The other benefit provided by 3D porous structure is that abundant pores in the co-deposited film could provide buffered spaces to accommodate volume expansion of silicon during the charge and discharge processes so that the mechanical stress of the film can be alleviated to ensure a good adhesion and thus a long cycling life. By comparison with the EPD co-deposited film, the conventional film (Figure 3e,f) exhibits a completely different morphology. It is much denser; the voids between the particles are much smaller. The EDX mapping of the EPD co-deposited film for the elements Si, C, Cu (substrate) is shown in Figure 4. From these images, it is clear that both nano-Si and AB

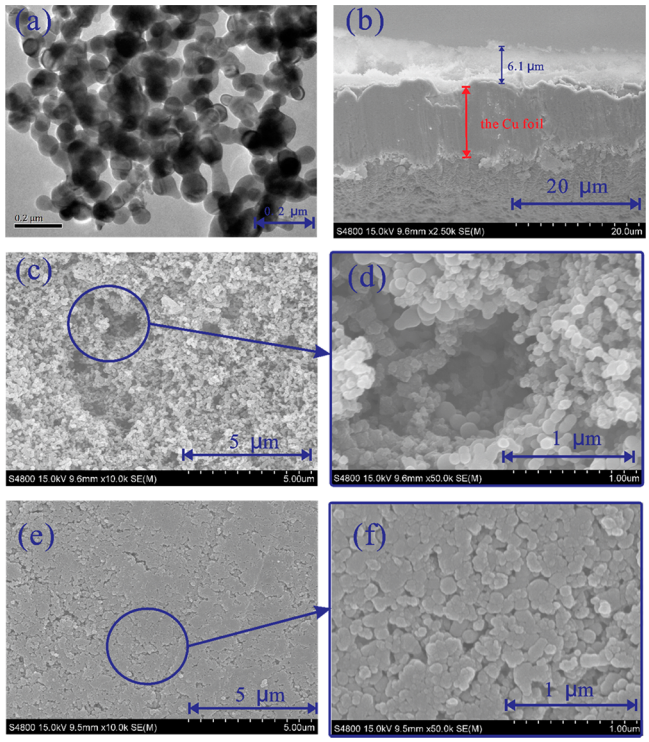

Figure 3. (a) TEM image of pristine nano-Si. (b) Cross-section SEM image of the co-deposited film for 5 s EPD duration. (c, d) SEM images of surface of the electrode fabricated by EPD method. (e, f) SEM image of surface of the electrode fabricated by the conventional method.

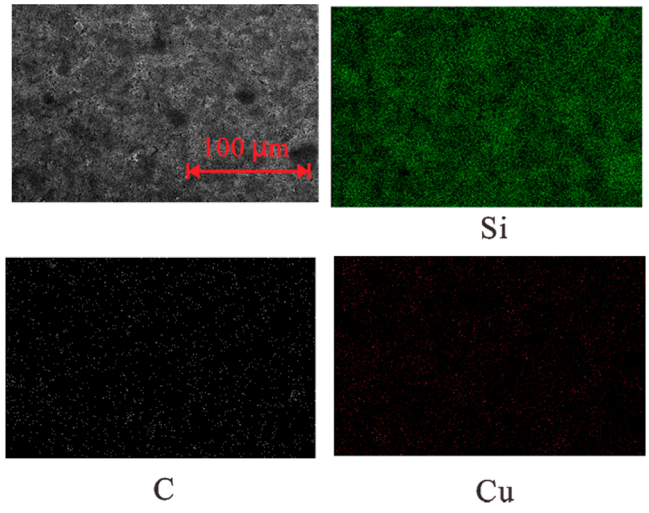

Figure 4. EDX images of the electrode fabricated by EPD method.

particles are uniformly deposited on the Cu foil to form a homogeneous co-deposited film. On the basis of the element analysis, the compositions of the nano-Si and AB are calculated to be 89.10% and 10.90%, respectively.

EPD is a physical process; thus, it should not change the crystal structure of nano-Si particles, which was confirmed by XRD analysis of the co-deposited film as shown in Figure 5. The XRD pattern of co-deposited film (Figure 5a) is exactly the same as that of pristine nano-Si powder (Figure 5b) after subtracting the contribution from copper foil, and they are both consistent well with the standard XRD data of Si (JCPDS no.01-070-3038).

DOI: 10.1021/acsami.5b00421
ACS Appl. Mater. Interfaces 2015, 7, 7497−7504

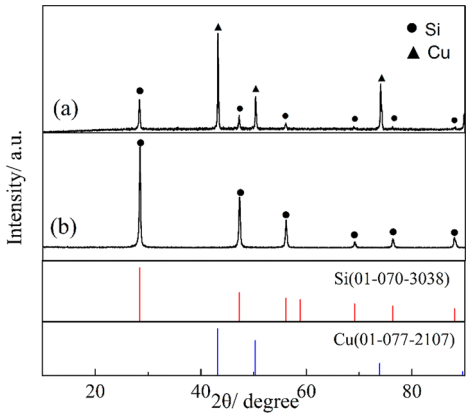

Figure 5. XRD patterns of (a) co-deposited film formed on Cu foil by EPD method and (b) pristine nano-Si powder.

EPD is a simple yet powerful technology to prepare a dense film starting from nanoparticles.[30] As EPD process progresses, the concentrations of both nanoparticles will change and the reaction rate will easily become diffusion controlled; thus, we applied slow magnetic stirring to keep the concentrations of both particles approximately unchanged during the deposition process by increase of convection and prevention of sedimentation. With all other parameters kept unchanged (concentrations, electrical filed strength, stirring speed, etc.), we studied the growth kinetic of nano-Si and AB co-deposited film on Cu foil by varying deposition duration, which is shown in Figure 6. From this graph, we can see that the mass of the

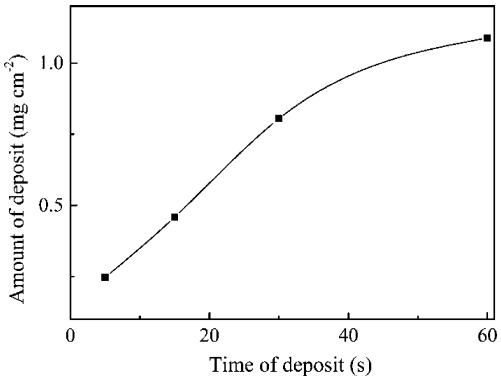

Figure 6. EPD kinetic curve of nano-Si and AB deposited on Cu foil.

deposit film increases linearly within 30 s; after that it slowly reaches the saturation point around 60 s. When the deposition time is more than 60 s, however, we observed that the co-deposited film became flaky, and some powder starts to fall off from the surface. Hence the deposition time is limited within 60 s. Even though the deposition time is 5 s, the load mass of the nano-Si and AB composite in the film is about 0.25 mg·cm^{-2}, meaning its theoretical capacity is close to 1 mAh·cm^{-2}, which is higher than many binder-free thin film electrodes fabricated via radio frequency magnetron sputtering technology.[33,34]

The nano-Si and AB EPD co-deposit films with different duration times exhibit quite different electrochemical performances as shown in Figure 7, and more details are summarized in Table 3. All the electrodes were cycled at 0.1 C with the voltage range of 0.02−1.5 V (vs Li$^+$/Li). The discharge capacity retention is obtained by using the discharge capacity after 50

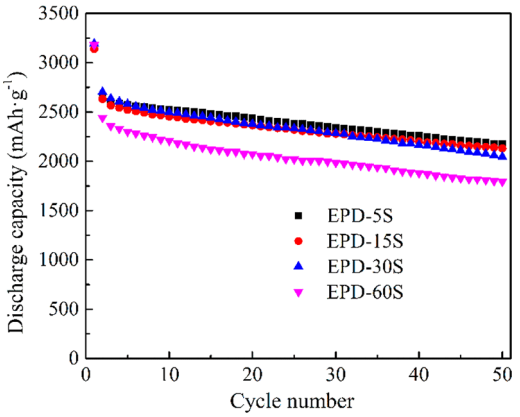

Figure 7. Cycling performance of electrodes fabricated by EPD method with different deposition time at 0.1 C.

cycles to divide the second discharge capacity (the reversible discharge capacity). The Coulombic efficiencies of the first cycle of the electrodes fabricated by EPD method within 30s (named as EPD-5s, EPD-15s, EPD-30s) are all around 80%; their specific charge capacities of first cycle are 2520, 2528, and 2586 mAh·g^{-1}, and discharge capacity retention values are 82%, 81%, and 76% after 50 cycles, respectively. However, these characteristics of EPD-60s electrode are 74%, 2353 mAh g^{-1} and 73%, respectively, all are much lower than those of the electrodes prepared within 30 s. These differences agreed well with our observation that the film prepared with longer deposition time is flaky; thus, contacts between particles are much looser, which is detrimental to electronic conductivity and stability of the electrode. The cycling performance of the electrode with the deposition duration of 4s is similar to EPD-5s (Figure S2 and Figure S3 in the Supporting Information).

Upon the basis of the above physical and electrochemical data, EPD-5s electrode is selected to compare with the electrode prepared by the conventional method. Since mass/area value of nano-Si in EPD-5s electrode is 0.221 mg·cm^{-2}, the mass/area value of nano-Si in the conventional method electrode is controlled at 0.229 mg·cm^{-2} during the fabrication process to ensure that the comparison between these two electrodes is legit.

The EPD-5s electrode exhibits a typical discharge plateau of Si at around 0.4 V (vs Li/Li$^+$, Figure 8a).[35] The short discharge plateau at around 1.2 V in the first cycle can be attributed to the decomposition of the FEC additive in the electrolyte.[36] The following long slope can be ascribed to the formation of Li−Si alloys.[37,38] EPD-5s electrode exhibits an initial charge/discharge capacity of 2520/3150 mAh·g^{-1}, respectively, and a much improved first Coulombic efficiency of 80% as compared with 64% for the conventional method electrode.

The CVs for the first five cycles of EPD-5s (Figure 8b) were found to be similar to that of the conventional method electrode (Figure S4 in the Supporting Information). For the cathodic processes, the broad peak centered at 0.22−0.24 V might be attributed to the formation of a series of Li−Si alloy (Li_xSi).[39,40] The sharp peak close to 0.02 V could be attributed to the phase transition of Li_xSi to $Li_{15}Si_4$.[41] For the anodic processes, there are two broad peaks in the potential range of 0.35−0.53 V which would be attributed to the delithiation reaction of Li−Si phases.[42] The intensities of both cathodic and anodic peaks gradually increase with charge/discharge because

DOI: 10.1021/acsami.5b00421
ACS Appl. Mater. Interfaces 2015, 7, 7497−7504

Table 3. Electrochemical Properties of Electrodes Fabricated by EPD Method with Different Deposition Time at 0.1 C

sample	first discharge capacity, mAh·g^{-1}	first charge capacity, mAh·g^{-1}	first Columbic efficiency, %	discharge capacity after 50 cycles, mAh·g^{-1}	discharge capacity retention after 50 cycles, %
EPD-5s	3150	2520	80	2175	82
EPD-15s	3141	2528	80	2131	81
EPD-30s	3193	2586	81	2047	76
EPD-60s	3180	2353	74	1794	73

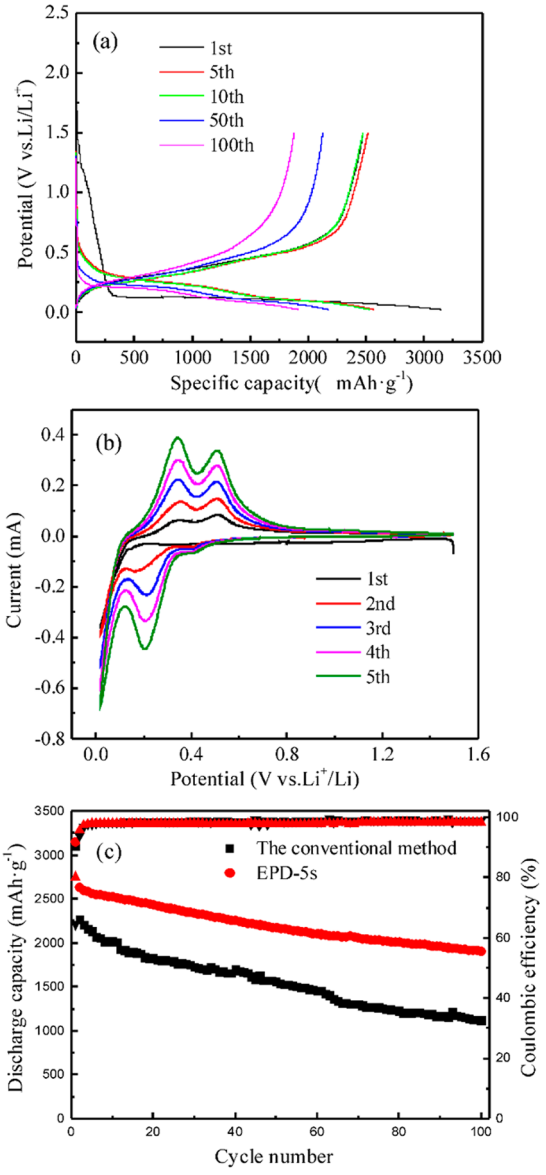

Figure 8. (a) Galvanostatic charge−discharge curves of EPD-5s electrode. (b) Cyclic voltammetry profiles of EPD-5s electrode. (c) Charge−discharge curves of EPD-5s and the conventional method electrode at 0.1 C.

of activation of crystal Si, which has been reported in previous studies.[43,44]

Figure 8c shows the comparisons of cycling performances and Coulombic efficiencies between EPD-5s and the conventional method electrode at 0.1 C. The Coulombic efficiencies of the two electrodes increase gradually to an efficiency of 97% by the fifth cycle. From the 10th to the 100th cycle, both Columbic efficiency levels are as high as 98%. After 100 cycles, EPD-5s electrode exhibits a discharge capacity of 1913 mAh·g^{-1} with a discharge capacity retention of 73%. On the other hand, the conventional method electrode only showed a discharge capacity of 1121 mAh·g^{-1} with a discharge capacity retention of 49%. A full cell made of $LiCoO_2$ cathode and EPD-5s anode was also investigated; the full cell has a charge capacity of 2034 mAh g^{-1} and retention of 79% after 30 cycles (Figures S5 and S6 in the Supporting Information). There might be two reasons for different performances of the two electrodes. First, the EPD method can provide a more effective mixed state between nano-Si and AB (see elemental mapping data). Second and probably the most important reason is that the porous structure of EPD-5s electrode could accommodate the volume change during lithium-ion insertion and extraction processes; thereby EPD-5s electrode is more mechanically stable and exhibits better cycling stability than the conventional method electrode.

Figure 9 shows cycling performance of EPD-5s and the conventional method electrode at various current rates. More

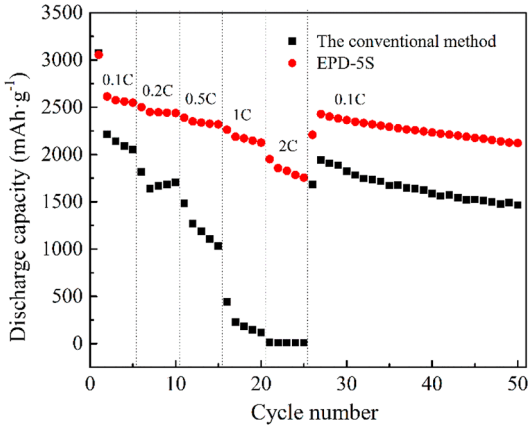

Figure 9. Cycling performance of EPD-5s and the conventional method electrode at various current rates.

details are summarized in Table 4. The cells were cycled at 0.1 C for the initial five cycles. Then the current density was raised gradually to 2 C and finally returned to 0.1 C again. At each current density five cycles were performed. For EPD-5s. It showed the initial discharge capacity of 3151 mAh·g^{-1}. At 0.2 C it exhibited an average discharge capacity of 2520 mAh·g^{-1}. At higher current densities of 0.5, 1, and 2 C, the average discharge capacity showed 2426, 2238, and 1890 mAh·g^{-1}, respectively, when reducing the current density back to 0.1 C again. The discharge capacity raised to 2504 mAh·g^{-1}. However, for the conventional method, it only exhibited an average discharge capacity of 1701, 1228, 215, and 11 mAh·g^{-1} at 0.2, 0.5, 1, and 2 C, respectively. This result reveals the better recovery of EPD-5s after 20 cycles of high current rates.

Figure 10 shows Nyquist plots of the EPD and conventional electrodes. Both samples were tested after 20 discharge−charge cycles. The impedance curves show one compressed semicircle

DOI: 10.1021/acsami.5b00421
ACS Appl. Mater. Interfaces 2015, 7, 7497−7504

Table 4. Electrochemical Properties of EPD-5s and the Conventional Method Electrode at Various Current Rates

sample	first discharge capacity, mAh g^{-1}	average discharge capacity at 0.2 C, mAh g^{-1}	average discharge capacity at 0.5 C, mAh g^{-1}	average discharge capacity at 1 C, mAh g^{-1}	average discharge capacity at 2 C, mAh g^{-1}
conventional method	3071	1701	1228	215	11
EPD-5s	3151	2520	2426	2238	1890

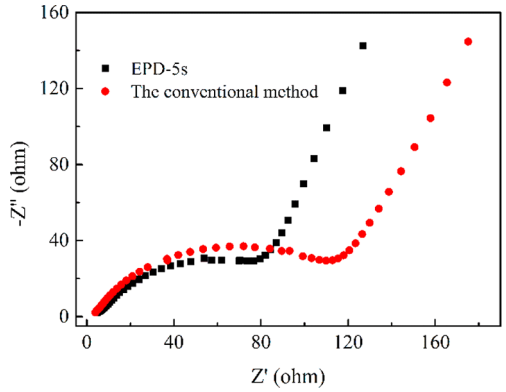

Figure 10. Nyquist plots of the EPD and conventional electrodes after 20 cycles.

in the medium-frequency region, which could be assigned to the charge transfer resistance (Rct), and an inclined line in the low-frequency range, which could be considered as Warburg impedance.[45−47] The Rct is calculated to be 48.07 and 114.3 Ω·cm^{-2} for the EPD and conventional electrode, respectively. EPD-5s electrode exhibited a smaller Rct than the conventional method electrode, indicating the enhanced ionic conductivity of EPD electrode.

The cycle life of both the EPD and conventional electrodes at high current densities is shown in Figure 11. These cells were

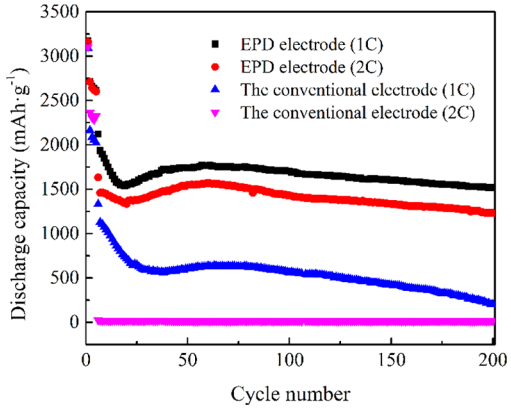

Figure 11. Long-term rate performance of EPD-5s and the conventional method electrode at high current densities.

first cycled at 0.1 C for the initial five cycles. Then the current density was increased to 1 and 2 C for 200 cycles, respectively. EPD-5s exhibited a discharge capacity of 1516 mAh·g^{-1} at 1 C and 1231 mAh·g^{-1} at 2 C after 200 cycles, respectively, while the conventional electrode only showed much lower capacities of 204 and 14 mAh·g^{-1} after 200 cycles. Thus, the EPD electrodes are much superior to conventional electrode. This superiority is attributed to the 3D porous structure of electrode fabricated by EPD method: one is that the electrode has a higher specific surface area, resulting in the shorter diffusion path for lithium ions and improvement of transport between electrode and electrolyte of lithium ions for better rate capability. Two is that the higher is the porosity of the electrode, the more void space to accommodate volume change of the electrode during cycling, thus more mechanically stable electrode to enable a longer cycle life. This can be clearly deduced from the SEM images of the conventional and EPD deposited film after cycling, shown in Figure 12. Both

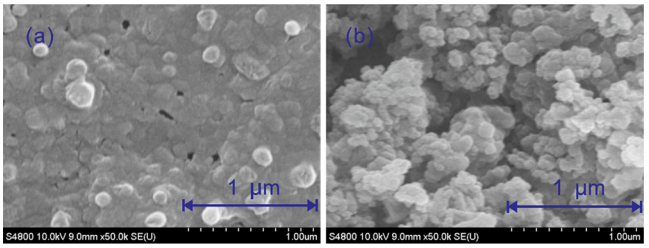

Figure 12. SEM images of (a) the conventional film after 100 cycles at 0.1C and (b) the EPD co-deposited film after 100 cycles at 0.1 C.

electrodes after cycling were covered with SEI films, but the surface morphologies of the electrodes are quite different: in the conventional electrode, its SEI film is rather smooth and with very few voids. By contrast, the surface of EPD electrode is still very rough and many voids are still present in the electrode even after 100 cycles.

The absence of binder in the EPD electrode also allows more straightforward analysis of the SEI. On the basis of the XPS data (see Figure S7), the SEI layer is mainly composed of Li_2CO_3, $ROCO_2Li$, LiF, and $LiPF_6$. These species are consistent with previous studies.[48−50]

On the basis of these data, we believe that the EPD method can be a power tool to prepare silicon thin film electrode to overcome its volume expansion/contraction issue for realization of silicon electrode potential in real industrial applications.

4. CONCLUSION

We demonstrated here that a binder-free Si nanoparticle electrode for LIB can be successfully fabricated by simper yet versatile one-step EPD process. Surface modified nanosized Si and AB particles are bonded tightly together to form a 3D porous structured thin film electrode on copper substrate through the EPD process. Our results demonstrate that with careful control of the co-deposition parameter, we can produce EPD electrode with much improved electrochemical performance, such as higher capacity, longer cycle life, and better rate capability. These improvements stem from the 3D porous structure of the electrode. The 3D porous structure of the electrode is beneficial to alleviate volume expansion of silicon during the charge and discharge processes and facilitate faster transport kinetics of lithium ions, which leads to better cycling and rate performances.

DOI: 10.1021/acsami.5b00421
ACS Appl. Mater. Interfaces 2015, 7, 7497−7504

■ ASSOCIATED CONTENT

Supporting Information

Photographs of EPD-5S electrode after 100 cycles; Henry equation; direct optical photographs of EPD-2s, EPD-3s, and EPD-4s electrodes; cycling performance of EPD-4s and EPD-5s electrodes; cyclic voltammetry profiles of the conventional method electrode; cycling performance and galvanostatic charge−discharge curves of full cell made of $LiCoO_2$ cathode and EPD-5s anode at 0.1 C; XPS spectra of EPD-5s electrode after one cycle. This material is available free of charge via the Internet at http://pubs.acs.org.

■ AUTHOR INFORMATION

Corresponding Author

*E-mail: jbzhao@xmu.edu.cn.

Notes

The authors declare no competing financial interest.

■ ACKNOWLEDGMENTS

The authors gratefully acknowledge the financial support from the National High Technology Research and Development Program of China (Grant 2012AA110204), National Natural Science Foundation of China (Grant 21321062), and Key Project of Science and Technology of Xiamen (Grant 2013H6022).

■ REFERENCES

(1) Chan, C. K.; Patel, R. N.; O'Connell, M. J.; Korgel, B. A.; Cui, Y. Solution-Grown Silicon Nanowires for Lithium-Ion Battery Anodes. *ACS Nano* **2010**, *4*, 1443−1450.

(2) Wang, J. W.; He, Y.; Fan, F.; Liu, X. H.; Xia, S.; Liu, Y.; Harris, C. T.; Li, H.; Huang, J. Y.; Mao, S. X.; Zhu, T. Two-Phase Electrochemical Lithiation in Amorphous Silicon. *Nano Lett.* **2013**, *13*, 709−715.

(3) Zhang, W.-J. A Review of the Electrochemical Performance of Alloy Anodes for Lithium-Ion Batteries. *J. Power Sources* **2011**, *196*, 13−24.

(4) Boukamp, B. A.; Lesh, G. C.; Huggins, R. A. All-Solid Lithium Electrodes with Mixed-Conductor Matrix. *J. Electrochem. Soc.* **1981**, *128*, 725−729.

(5) Liu, N.; Wu, H.; McDowell, M. T.; Yao, Y.; Wang, C. M.; Cui, Y.; Yolk-Shell, A. Design for Stabilized and Scalable Li-Ion Battery Alloy Anodes. *Nano Lett.* **2012**, *12*, 3315−3321.

(6) Park, M. H.; Kim, M. G.; Joo, J.; Kim, K.; Kim, J.; Ahn, S.; Cui, Y.; Cho, J. Silicon Nanotube Battery Anodes. *Nano Lett.* **2009**, *9*, 3844−3847.

(7) Kim, H.; Han, B.; Choo, J.; Cho, J. Three-Dimensional Porous Silicon Particles for Use in High-Performance Lithium Secondary Batteries. *Angew. Chem., Int. Ed.* **2008**, *47*, 10151−10154.

(8) Chen, Y.; Nie, M.; Lucht, B. L.; Saha, A.; Guduru, P. R.; Bose, A. High Capacity, Stable Silicon/Carbon Anodes for Lithium-Ion Batteries Prepared Using Emulsion-Templated Directed Assembly. *ACS Appl. Mater. Interfaces* **2014**, *6*, 4678−83.

(9) He, M.; Sa, Q.; Liu, G.; Wang, Y. Caramel Popcorn Shaped Silicon Particle with Carbon Coating as a High Performance Anode Material for Li-Ion Batteries. *ACS Appl. Mater. Interfaces* **2013**, *5*, 11152−11158.

(10) Li, H.; Huang, X.; Chen, L.; Wu, Z.; Liang, Y. A High Capacity Nano-Si Composite Anode Material for Lithium Rechargeable Batteries. *Electrochem. Solid-State Lett.* **1999**, *2*, 547−549.

(11) Chan, C. K.; Peng, H.; Liu, G.; McIlwrath, K.; Zhang, X. F.; Huggins, R. A.; Cui, Y. High-Performance Lithium Battery Anodes Using Silicon Nanowires. *Nat. Nanotechnol.* **2008**, *3*, 31−35.

(12) Kim, H.; Cho, J. Superior Lithium Electroactive Mesoporous Si@Carbon Core-Shell Nanowires for Lithium Battery Anode Material. *Nano Lett.* **2008**, *8*, 3688−3691.

(13) Hassan, F. M.; Elsayed, A. R.; Chabot, V.; Batmaz, R.; Xiao, X.; Chen, Z. Subeutectic Growth of Single-Crystal Silicon Nanowires Grown on and Wrapped with Graphene Nanosheets: High-Performance Anode Material For Lithium-Ion Battery. *ACS Appl. Mater. Interfaces* **2014**, *6*, 13757−13764.

(14) Lim, K. W.; Lee, J. I.; Yang, J.; Kim, Y. K.; Jeong, H. Y.; Park, S.; Shin, H. S. Catalyst-Free Synthesis of Si-SiOx Core-Shell Nanowire Anodes for High-Rate and High-Capacity Lithium-Ion Batteries. *ACS Appl. Mater. Interfaces* **2014**, *6*, 6340−6345.

(15) Ohara, S.; Suzuki, J.; Sekine, K.; Takamura, T.; Thin Film, A. Silicon Anode for Li-Ion Batteries Having a Very Large Specific Capacity and Long Cycle Life. *J. Power Sources* **2004**, *136*, 303−306.

(16) Kim, J. B.; Jun, B. S.; Lee, S. M. Improvement of Capacity and Cyclability of Fe/Si Multilayer Thin Film Anodes for Lithium Rechargeable Batteries. *Electrochim. Acta* **2005**, *50*, 3390−3394.

(17) Yu, Y.; Yue, C.; Sun, S.; Lin, W.; Su, H.; Xu, B.; Li, J.; Wu, S.; Li, J.; Kang, J. The Effects of Different Core-Shell Structures on the Electrochemical Performances of Si-Ge Nanorod Arrays as Anodes for Micro-Lithium Ion Batteries. *ACS Appl. Mater. Interfaces* **2014**, *6*, 5884−5890.

(18) Besra, L.; Liu, M. A Review on Fundamentals and Applications of Electrophoretic Deposition (EPD). *Prog. Mater. Sci.* **2007**, *52*, 1−61.

(19) Ui, K.; Funo, S.-y.; Nagase, H.; Idemoto, Y.; Koura, N. Fabrication of Binder-Free Positive Electrode for Li-Ion Secondary Batteries by Electrophoretic Deposition Method. *Electrochemistry (Tokyo, Jpn.)* **2006**, *74*, 474−478.

(20) Kanamura, K.; Goto, A.; Hamagami, J. i.; Umegaki, T. Electrophoretic Fabrication of Positive Electrodes for Rechargeable Lithium Batteries. *Electrochem. Solid-State Lett.* **2000**, *3*, 259−262.

(21) Caballero, A.; Hernán, L.; Melero, M.; Morales, J.; Moreno, R.; Ferrari, B. $LiNi_{0.5}Mn_{1.5}O_4$ Thick-Film Electrodes Prepared by Electrophoretic Deposition for Use in High Voltage Lithium-Ion Batteries. *J. Power Sources* **2006**, *158*, 583−590.

(22) Ui, K.; Kawamura, S.; Kumagai, N. Fabrication of Binder-Free SnO_2 Nanoparticle Electrode for Lithium Secondary Batteries by Electrophoretic Deposition Method. *Electrochim. Acta* **2012**, *76*, 383−388.

(23) Rangasamy, B.; Hwang, J. Y.; Choi, W. Multi Layered Si-CuO Quantum Dots Wrapped by Graphene for High-Performance Anode Material in Lithium-Ion Battery. *Carbon* **2014**, *77*, 1065−1072.

(24) Wu, P.; Wang, H.; Tang, Y.; Zhou, Y.; Lu, T. Three-Dimensional Interconnected Network of Graphene-Wrapped Porous Silicon Spheres: In Situ Magnesiothermic-Reduction Synthesis and Enhanced Lithium-Storage Capabilities. *ACS Appl. Mater. Interfaces* **2014**, *6*, 3546−3552.

(25) Zhu, Q.; Wu, P.; Zhang, J.; Zhang, W.; Zhou, Y.; Tang, Y.; Lu, T. Cyanogel-Derived Formation of 3 D Nanoporous SnO_2-M_xO_y (M=Ni, Fe, Co) Hybrid Networks for High-Performance Lithium Storage. *ChemSusChem* **2015**, *8*, 131−137.

(26) Li, J.; Wu, P.; Tang, Y.; Xu, X.; Zhou, Y.; Chen, Y.; Lu, T. Three-Dimensional Mesoporous Sn-Ni@C Network Derived from Cyanogel Coordination Polymers: Towards High-Performance Anodes for Lithium Storage. *CrystEngComm* **2013**, *15*, 10340−10345.

(27) Hidber, P. C.; Graule, T. J.; Gauckler, L. J. Citric Acid—A Dispersant for Aqueous Alumina Suspensions. *J. Am. Ceram. Soc.* **1996**, *79*, 1857−1867.

(28) Hidber, P. C.; Graule, T. J.; Gauckler, L. J. Competitive Adsorption of Citric-Acid and Poly(vinyl alcohol) onto Alumina and Its Influence on the Binder Migration during Drying. *J. Am. Ceram. Soc.* **1995**, *78*, 1775−1780.

(29) Fazio, S.; Guzman, J.; Colomer, M.; Salomoni, A.; Moreno, R. Colloidal Stability of Nanosized Titania Aqueous Suspensions. *J. Eur. Ceram. Soc.* **2008**, *28*, 2171−2176.

(30) Dickerson, J. H.; Boccaccini, A. R. *Electrophoretic Deposition of Nanomaterials*; Springer: New York, 2012.

(31) Kruger, H. G.; Knote, A.; Schindler, U.; Kern, H.; Boccaccini, A. R. Composite Ceramic-Metal Coatings by Means of Combined Electrophoretic Deposition and Galvanic Methods. *J. Mater. Sci.* **2004**, *39*, 839−844.

DOI: 10.1021/acsami.5b00421
ACS Appl. Mater. Interfaces 2015, 7, 7497−7504

(32) Corni, I.; Ryan, M. P.; Boccaccini, A. R. Electrophoretic Deposition: From Traditional Ceramics to Nanotechnology. *J. Eur. Ceram. Soc.* **2008**, *28*, 1353−1367.
(33) Wu, C.-H.; Hung, F.-Y.; Lui, T.-S.; Chen, L.-H. Microstructures and the Charge-Discharge Characteristics of Advanced Al-Si Thin Film Materials. *Mater. Trans.* **2010**, *51*, 1958−1963.
(34) Datta, M. K.; Maranchi, J.; Chung, S. J.; Epur, R.; Kadakia, K.; Jampani, P.; Kumta, P. N. Amorphous Silicon-Carbon Based Nano-Scale Thin Film Anode Materials for Lithium Ion Batteries. *Electrochim. Acta* **2011**, *56*, 4717−4723.
(35) Shao, D.; Tang, D.; Mai, Y.; Zhang, L. Nanostructured Silicon/Porous Carbon Spherical Composite as a High Capacity Anode for Li-Ion Batteries. *J. Mater. Chem. A* **2013**, *1*, 15068−15075.
(36) Mogi, R.; Inaba, M.; Jeong, S.-K.; Iriyama, Y.; Abe, T.; Ogumi, Z. Effects of Some Organic Additives on Lithium Deposition in Propylene Carbonate. *J. Electrochem. Soc.* **2002**, *149*, A1578−A1583.
(37) Zheng, Y.; Yang, J.; Wang, J.; NuLi, Y. Nano-Porous Si/C Composites for Anode Material of Lithium-Ion Batteries. *Electrochim. Acta* **2007**, *52*, 5863−5867.
(38) Wang, M.-S.; Fan, L.-Z.; Huang, M.; Li, J.; Qu, X. Conversion of Diatomite to Porous Si/C Composites as Promising Anode Materials for Lithium-Ion Batteries. *J. Power Sources* **2012**, *219*, 29−35.
(39) Huang, X.; Pu, H.; Chang, J.; Cui, S.; Hallac, P. B.; Jiang, J.; Hurley, P. T.; Chen, J. Improved Cyclic Performance of Si Anodes for Lithium-Ion Batteries by Forming Intermetallic Interphases between Si Nanoparticles and Metal Microparticles. *ACS Appl. Mater. Interfaces* **2013**, *5*, 11965−11970.
(40) Jiang, T.; Zhang, S.; Qiu, X.; Zhu, W.; Chen, L. Preparation and Characterization of Silicon-Based Three-Dimensional Cellular Anode for Lithium Ion Battery. *Electrochem. Commun.* **2007**, *9*, 930−934.
(41) Hatchard, T. D.; Dahn, J. R. In Situ XRD and Electrochemical Study of the Reaction of Lithium with Amorphous Silicon. *J. Electrochem. Soc.* **2004**, *151*, A838−A842.
(42) Luais, E.; Sakai, J.; Desplobain, S.; Gautier, G.; Tran-Van, F.; Ghamouss, F. Thin and Flexible Silicon Anode Based on Integrated Macroporous Silicon Film onto Electrodeposited Copper Current Collector. *J. Power Sources* **2013**, *242*, 166−170.
(43) Ge, M.; Rong, J.; Fang, X.; Zhou, C. Porous Doped Silicon Nanowires for Lithium Ion Battery Anode with Long Cycle Life. *Nano Lett.* **2012**, *12*, 2318−2323.
(44) Hassan, F. M.; Chabot, V.; Elsayed, A. R.; Xiao, X.; Chen, Z. Engineered Si Electrode Nanoarchitecture: A Scalable Postfabrication Treatment for the Production of Next-Generation Li-Ion Batteries. *Nano Lett.* **2014**, *14*, 277−283.
(45) Sun, W.; Hu, R. Z.; Liu, H.; Zeng, M. Q.; Yang, L. C.; Wang, H. H.; Zhu, M. Embedding Nano-Silicon in Graphene Nanosheets by Plasma Assisted Milling for High Capacity Anode Materials in Lithium Ion Batteries. *J. Power Sources* **2014**, *268*, 610−618.
(46) Chen, D.; Yi, R.; Chen, S.; Xu, T.; Gordin, M. L.; Wang, D. Facile Synthesis of Graphene-Silicon Nanocomposites with an Advanced Binder for High-Performance Lithium-Ion Battery Anodes. *Solid State Ionics* **2014**, *254*, 65−71.
(47) Chou, S. L.; Wang, J. Z.; Choucair, M.; Liu, H. K.; Stride, J. A.; Dou, S. X. Enhanced Reversible Lithium Storage in a Nanosize Silicon/Graphene Composite. *Electrochem. Commun.* **2010**, *12*, 303−306.
(48) Nie, M. Y.; Abraham, D. P.; Chen, Y. J.; Bose, A.; Lucht, B. L. Silicon Solid Electrolyte Interphase (SEI) of Lithium Ion Battery Characterized by Microscopy and Spectroscopy. *J. Phys. Chem. C* **2013**, *117*, 13403−13412.
(49) Nakai, H.; Kubota, T.; Kita, A.; Kawashima, A. Investigation of the Solid Electrolyte Interphase Formed by Fluoroethylene Carbonate on Si Electrodes. *J. Electrochem. Soc.* **2011**, *158*, A798−A801.
(50) Chen, L. B.; Wang, K.; Xie, X. H.; Xie, J. Y. Effect of Vinylene Carbonate (VC) as Electrolyte Additive on Electrochemical Performance of Si Film Anode for Lithium Ion Batteries. *J. Power Sources* **2007**, *174*, 538−543.

DOI: 10.1021/acsami.5b00421
ACS Appl. Mater. Interfaces 2015, 7, 7497−7504